# Highly Robust, Recyclable Displacement Assay for Mercuric Ions in Aqueous Solutions and Living Cells

**Dingbin Liu,[†,‡,§] Shouju Wang,[‡] Magdalena Swierczewska,[‡] Xinglu Huang,[‡,§] Ashwinkumar A. Bhirde,[‡] Jiashu Sun,[⊥] Zhuo Wang,[⊥] Min Yang,[†,*] Xingyu Jiang,[⊥,*] and Xiaoyuan Chen[‡,*]**

[†]Key Laboratory of Nuclear Medicine, Ministry of Health, Jiangsu Key Laboratory of Molecular Nuclear Medicine, Jiangsu Institute of Nuclear Medicine, Wuxi, Jiangsu 214063, China, [‡]Laboratory of Molecular Imaging and Nanomedicine (LOMIN), National Institute of Biomedical Imaging and Bioengineering (NIBIB), National Institutes of Health (NIH), Bethesda, Maryland 20892, United States, [⊥]CAS Key Lab for Biological Effects of Nanomaterials and Nanosafety, National Center for NanoScience and Technology, 11 Beiyitiao, ZhongGuanCun, Beijing 100190, China, and [§]Center for Molecular Imaging and Translational Medicine, School of Public Health, Xiamen University, Xiamen 361005, China

**ABSTRACT** We designed a recyclable $Hg^{2+}$ probe based on Rhodamine B isothiocyanate (RBITC)-poly(ethylene glycol) (PEG)-comodified gold nanoparticles (AuNPs) with excellent robustness, selectivity, and sensitivity. On the basis of a rational design, only $Hg^{2+}$ can displace RBITC from the AuNP surfaces, resulting in a remarkable enhancement of RBITC fluorescence initially quenched by AuNPs. To maintain stability and monodispersity of AuNPs in real samples, thiol-terminated PEG was employed to bind with the remaining active sites of AuNPs. Besides, this displacement assay can be regenerated by resupplying free RBITC into the AuNPs solutions that were already used for detecting $Hg^{2+}$. Importantly, the detection limit of this assay for $Hg^{2+}$ (2.3 nM) was lower than the maximum limits guided by the United States Environmental Protection Agency as well as that permitted by the World Health Organization. The efficiency of this probe was demonstrated in monitoring $Hg^{2+}$ in complex samples such as river water and living cells.

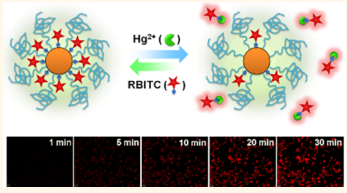


**KEYWORDS:** gold nanoparticles · sensitivity · selectivity · recyclable detection · Rhodamine B isothiocyanate

This study provides a highly robust and recyclable gold nanoparticle (AuNP)-based displacement assay for mercuric ions ($Hg^{2+}$) in aqueous solutions and living cells with ultrahigh selectivity and sensitivity. Mercury contamination is an ongoing public concern because inorganic $Hg^{2+}$ in contaminated water and soil can be transformed into methylmercury and accumulate in the human body through the food chain, posing severe threats to both human health and natural ecosystems.[1] Long-term exposure to high $Hg^{2+}$ levels can lead to serious and permanent damage to the central nervous system and other organs such as heart, kidneys, lungs, etc.[2,3] Standard methods for monitoring trace $Hg^{2+}$ include atomic absorption spectroscopy (AAS),[4] inductively coupled plasma-mass spectrometry (ICPMS),[5] and mass spectroscopy (MS).[6] Although these methods are sensitive and powerful, they require sophisticated instruments and specialized personnel to carry out the operational procedures. Moreover, time-consuming sample preparation and tedious preconcentration procedures are also involved. During the past decade, researchers have devoted considerable effort to the development of simple $Hg^{2+}$ probes, mainly based on fluorescent chemosensors using small organic molecules,[7] polymeric materials,[8] oligonucleotides,[9] and proteins.[10] Most of these systems, however, have limitations with respect to lack of water solubility, cross-reactivity with other metal ions, and short emission wavelengths. Therefore, it is extremely important to develop simple, inexpensive, highly sensitive and selective $Hg^{2+}$ probes that can provide real-time measurement of $Hg^{2+}$ levels in environmental and biological samples.

In the past two decades, tremendous progress in the design of high-sensitivity sensors has been made as a result of the development of nanotechnology. Particularly, AuNP-based fluorescence assays have drawn considerable research interest, because AuNPs are a unique quencher for fluorescent dyes through energy-transfer and electron-transfer processes.[11,12]

* Address correspondence to yangmin@jsinm.org, xingyujiang@nanoctr.cn, shawn.chen@nih.gov.

Received for review October 5, 2012 and accepted November 2, 2012.

**Published online November 02, 2012**
10.1021/nn3046192

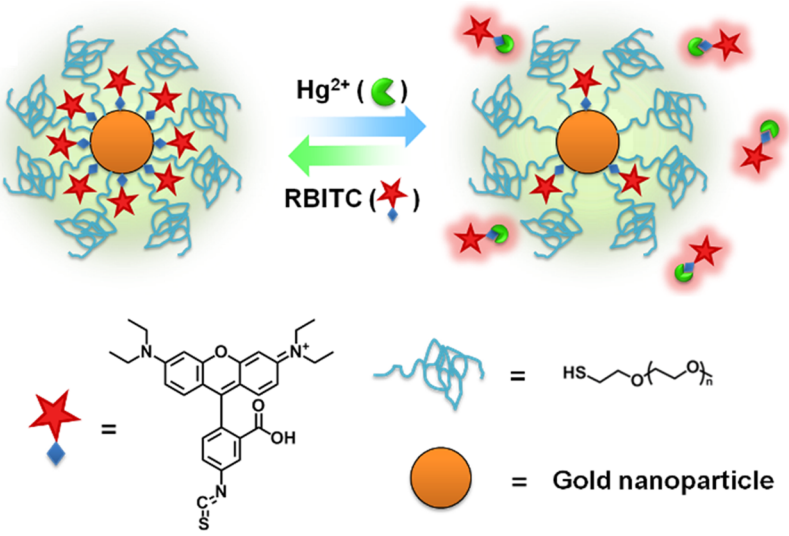


**Figure 1. Schematic illustration of the design for detecting $Hg^{2+}$ ions in a recyclable way.**

The extremely high quenching efficiencies of AuNPs (up to 99.8%[13,14]) make them very useful in numerous fluorescence-based assays for analytes.[15−20] For example, when Rhodamine B (RB) fluorescent dye molecules adsorb onto AuNP surfaces, their fluorescence is efficiently quenched by AuNPs. Upon addition of $Hg^{2+}$, RBs are displaced from the AuNP surfaces to recover their fluorescence.[15,16] The sensitivity of these assays is higher than those reported by using conventional colorimetric assays. However, the selectivity of these assays is so poor that it makes them unlikely to detect $Hg^{2+}$ by the RB-AuNP system alone. To improve selectivity, pretreatment with thiol ligands and addition of masking agent (2,6-pyridinedicarboxylic acid, PDCA) were required.[15,16] The pretreatment of AuNPs and involvement of masking agent make these assays laborious and time-consuming and thus unsuitable for real-time detection of $Hg^{2+}$. Additionally, most AuNP-based assays fail to precisely determine targeted analytes in their native environments such as environmental samples and biological fluids because AuNPs tend to aggregate in real samples and thus are limited to pure aqueous solutions where $Hg^{2+}$ is added.[21] Therefore, it is vital to develop more stable, reliable and accurate detection methods with sufficient sensitivity and selectivity for $Hg^{2+}$ in real samples.

We herein design an improved, recyclable displacement assay for $Hg^{2+}$ detection for use in not only aqueous solutions but also living cells by using Rhodamine B isothiocyanate (RBITC)-poly(ethylene glycol) (PEG)-co-modified AuNPs (RBITC-PEG-AuNPs). The excellent selectivity of this assay for $Hg^{2+}$ over competing species can be expected by comparing the stability constant ($\log K_f$) of metallic ions with isothiocyanate (ITC, −N═C═S), a high-affinity anchoring groups commonly used to attach organic molecules to colloidal AuNPs. We note that the $\log K_f$ of $Hg(ITC)_n$ is ca. 21.8, whereas those of $Co^{2+}$, $Zn^{2+}$, $Cd^{2+}$, $Ni^{2+}$, $Pb^{2+}$, $Mn^{2+}$, $Fe^{2+}$, $Fe^{3+}$, $Cr^{3+}$, $Cu^{2+}$ and $Au^{+}$ are ca. 1.72, 2.0, 2.8, 1.76, 1.48, 1.23, 1.31, 4.64, 3.08, 10.4, and 16.98 respectively.[22] The $\log K_f$ of $Hg(ITC)_n$ is the only one that is larger than that of $Au(ITC)_n$, indicating that $Hg^{2+}$ has the highest affinity toward ITC. As a result, only $Hg^{2+}$ is capable of removing RBITC from the AuNP surface. The detachment of RBITC from AuNP surfaces induces the recovery of RBITC fluorescence that was initially quenched by AuNPs (Figure 1). After fluorescence detection, RBITC can be replenished on the AuNP surface, and the RBITC-PEG-AuNP platform can be used for additional rounds of $Hg^{2+}$ detection. To address instability of nanomaterials in native samples, we elegantly achieve monodispersity of RBITC-PEG-AuNPs in real detection conditions by functionalizing AuNP surfaces with thiol-terminated PEG. We previously reported that $Hg^{2+}$ is unable to remove thiol ligands from Au surfaces, except in extremely high acidic solutions (pH 1.0).[23] Therefore, after $Hg^{2+}$ is added to the detection assay, only RBITC can be displaced from the AuNP surfaces leaving PEG stably adsorbed on AuNPs for continued detection.

## RESULTS AND DISCUSSION

RBITC was chosen as the model fluorophore in this study because it is water-soluble, photostable, and strongly fluorescent. More importantly, AuNPs can be ideal energy acceptors quenching RBITC fluorescence *via* the nanoparticle surface energy transfer (NSET) effect.[11] RBITC molecules can tightly adsorb and anchor around AuNP surfaces by means of the strong affinity between the ITC group and Au.[24] In general, the most commonly used 13 nm AuNPs are prepared using a citrate reduction method and are stabilized by the negatively charged citrate. Upon addition of RBITC, the citrate, weakly adsorbed on Au surfaces, is replaced by RBITC molecules through Au−ITC bonds. It is worth noting that the metal−sulfur bond is found to be the

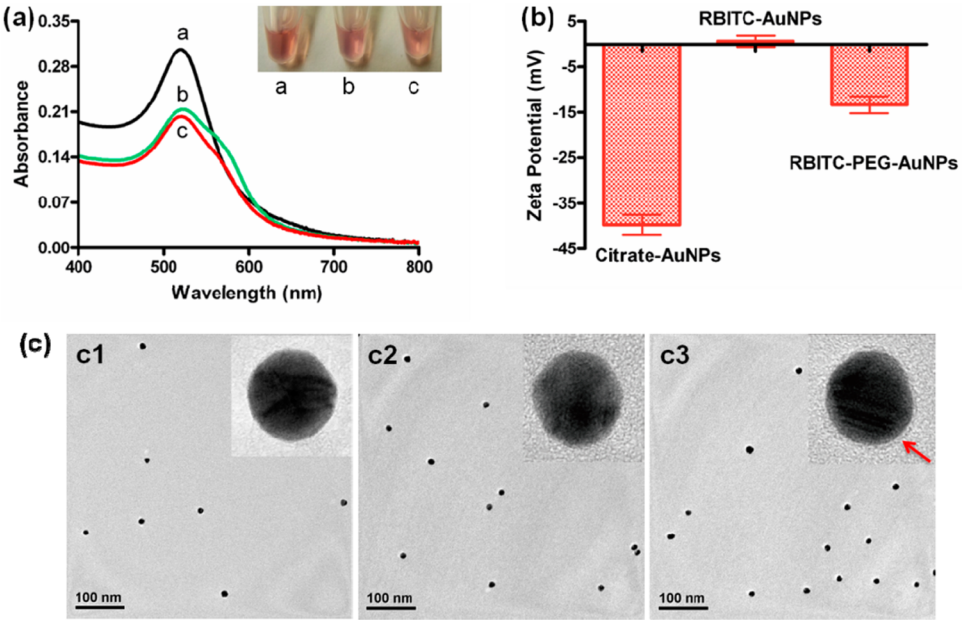


**Figure 2. (a) UV−vis spectra of citrate-AuNPs (a1), RBITC-AuNPs (a2) and RBITC-PEG-AuNPs (a3) and their corresponding solution colors. (b) Zeta potentials and (c) TEM images of citrate-AuNPs (c1), RBITC-AuNPs (c2), and RBITC-PEG-AuNPs (c3). High-resolution TEM was performed to analyze the organic layers surronding AuNPs. The red arrow indicates the PEG layer on the AuNP surface.**

strongest bond compared to other general functional chemical groups such as amines, carboxylic acids, phosphors, and alcohols. Therefore, the sulfur exchange method is the most common way to replace the original capping molecules and functionalize ligands onto Au surfaces.[25−27]

To utilize this assay in the real world, thiol-terminated PEG was subsequently added and adsorbed onto the remaining active sites of AuNPs *via* Au−S bond.[26] To confirm the quality of AuNPs after RBITC and PEG attachment, the AuNPs were characterized using UV−vis spectroscopy. As shown in Figure 2a, the as-prepared citrate-AuNPs solutions were red in color and showed a typical absorption band at 520 nm, which was attributed to the surface plasmon resonance of AuNPs whose size is about 13 nm.[23] The UV−vis spectra of RBITC-AuNPs and RBITC-PEG-AuNPs are similar to that of the citrate-AuNPs. The dominant absorption peak at 520 nm demonstrated proper dispersion of the 13-nm AuNPs, while the appearance of a new peak at roughly 555 nm was attributed to the RBITC absorbance of the RBITC-AuNP conjugates, which is similar to the other reported dye-AuNP systems.[28−30] We employed zeta potential measurements to further investigate the surface charge variations of AuNPs before and after functionalization (Figure 2b). As reported elsewhere, the charge of citrate-AuNPs is negative ($-39.7 \pm 3.8$ mV) because of the citric acid.[23,26,31] Once modified with RBITC, the zeta potential of AuNPs increased to be $0.7 \pm 2.2$ mV, most likely due to the copresence of the positively charged quaternary ammonium and the negatively charged carboxyl group in RBITC. After PEG adsorption on the remaining active sites of RBITC-AuNPs, the charge decreased to a negative value ($-13.3 \pm 3.2$ mV), owing to the huge amount of ethylene oxide units in PEG chains.[32−34] The surface functionalization was also supported by dynamic light scattering (DLS) data (Figure S1, Supporting Information). The average hydrodynamic diameter of RBITC-AuNPs was 21 nm (similar to the size of citrate-AuNPs), while that of the RBITC-PEG-AuNPs increased to 33 nm. In addition, the morphology of the functionalized AuNPs was determinated by transmission electron microscopy (TEM) (Figure 2c). By using high-resolution TEM, we can observe a thin organic layer that surrounds the AuNPs with an approximately 2−3 nm thickness (Figure 2c3), while the organic layers on citrate-AuNP and RBITC-AuNP surfaces were too thin to be observed.

If some citric acid is still adsorbed on RBITC-AuNPs, it will compete for binding with $Hg^{2+}$ and decrease the amount of $Hg^{2+}$ available to displace RBITC from the AuNP surfaces. As a consequence, the sensitivity of this displacement assay will decrease. Therefore, it is necessary to add excess RBITC into citrate-AuNPs solutions during the preparation of the AuNP-based probe to replace all of the citric acid on the AuNP. The amount of RBITC on AuNP surfaces can be quantitatively measured by comparing the absorbance changes of free RBITC before and after mixing with citrate-AuNPs and subsequently adding PEG. RBITC (10 $\mu$M) in pure water exhibits a typical fluorescence emission band at around 580 nm; with the addition of citrate-AuNPs, the intensity of the fluorescence peak decreased significantly by about 50% (Figure S2, Supporting Information). The phenomenon demonstrates the presence of the NSET

effect between AuNPs and RBITC. To quantify the amount of RBITC that attached onto AuNP surfaces, we measured the changes of UV−vis absorbance for excess, nonconjugated RBITC before and after mixing with citrate-AuNPs. With the assistance of a calibration curve of UV−vis absorbance versus RBITC concentrations (Figure S3, Supporting Information), the amount of attached RBITC per AuNP was calculated to be 1200. It is worth noting that the thiol-terminated PEG subsequently added may interact with Au, resulting in the subtraction of RBITC from Au surfaces. So we explored the appropriate reaction time and concentration of PEG. Figure S4, Supporting Information, shows the change of fluorescence intensities of RBITC solutions (10 $\mu$M) that were subsequently added with citrate-AuNPs (2.5 nM) and various concentrations of PEG (0−5 $\mu$M). The PEG functionality was recorded in 60 min. We observed that the fluorescence intensity for each solution increased significantly in 10 min and then displayed a very slow rise from 10 to 60 min. The absence of PEG was set as the control, whose fluorescence intensity had negligible change over time. We conclude that 10 min is sufficient for the PEG functionality of this system.

Next, we investigated the appropriate concentration of PEG by redissolving the RBITC-PEG-AuNPs pellets (functionalized by different concentrations of PEG) in phosphate-buffered saline (PBS). As shown in Figure S5, Supporting Information, when functionalizing RBITC-AuNPs with low concentrations (0, 1, 2 $\mu$M) of PEG, new absorption peaks appeared between 600 and 700 nm in the UV−vis spectra, indicating the formation of Au aggregates.[23,26] When we increased the PEG concentration to 3 $\mu$M, the RBITC-PEG-AuNPs remained well-dispersed in PBS. Therefore, we chose an optimized concentration of PEG (3 $\mu$M) for the modification, where AuNPs can be well-dispersed in high-salt solutions and simultaneously only a small number of RBITC (120 RBITC per AuNP) can be removed from the AuNP surfaces by PEG. In the process of preparing the RBITC-PEG-AuNPs, the absorbance changes of free RBITC in each step was monitored by UV−vis spectra (Figure S6, Supporting Information). The results show that the addition of such low concentrations of PEG (3 $\mu$M) caused just a few RBITC to be released from AuNP surfaces.

Most nanomaterial-based probes tend to aggregate in complex samples, thus reducing their efficiency and accuracy in monitoring targeted analytes. We herein evaluated the stability of this probe in various complex solutions and those with different pH values. The as-prepared RBITC-PEG-AuNPs were purified by centrifugation and the pellets were redissolved in various complex solutions including tap water, river water, PBS, and 10-fold concentrated PBS. Pure water was set as the control. We found that the color of the RBITC-PEG-AuNP solutions remained red even after standing for several hours, and correspondingly, the UV−vis spectra showed the typical absorption band for monodispersed AuNPs (Figure S7, Supporting Information). In contrast, the RBITC-AuNPs can only be redispersed in pure water. Upon mixing RBITC-AuNPs pellets with complex samples (including tap water, river water and PBS), the solution color changed from red to blue, indicating the formation of AuNP aggregates, which was confirmed by the appearance of a broad absorption peak at about 600 nm in the UV−visible spectrum (Figure S8, Supporting Information). The results reveal that RBITC-PEG-AuNPs can be stably monodispersed in various complex samples, enabling the use of this probe for real-world detection.

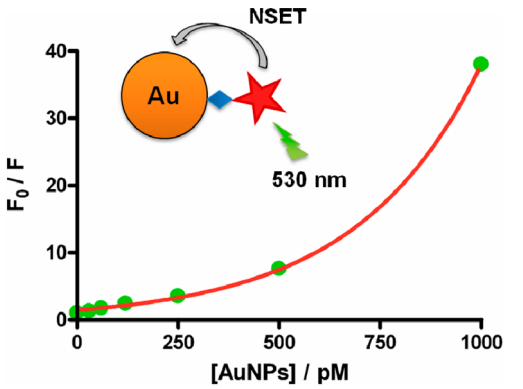


**Figure 3. Stern−Volmer plots of RBITC quenching by varying concentrations (0, 30, 60, 120, 250, 500, and 1000 pM) of AuNPs (13 nm).**

In addition, we evaluated if pH values could influence the monodispersity of RBITC-PEG-AuNPs. We utilized the plots of $A_{520}/A_{650}$ (the ratio of absorbance at 520 and 650 nm) versus various pH values to investigate the aggregation states of RBITC-PEG-AuNPs. Higher $A_{520}/A_{650}$ values indicate lower degrees of aggregation of AuNPs. Figure S9, Supporting Information, revealed that RBITC-PEG-AuNPs were well-dispersed in solutions ranging from pH 2.0 to 12.0, while RBITC-AuNPs only remained dispersed in pH 7.0−11.0 solutions. Based on this characterization, we can conclude that this nanosensor has the ability to detect $Hg^{2+}$ not only in various complex samples but also in solutions with a broad range of pH values.

We noted that the fluorescence intensity of RBITC (1 $\mu$M) decreased significantly after reaction with varying concentrations of citrate-AuNPs ranging from 0 to 1000 pM (Figure 3). More citrate-AuNPs resulted in higher-efficiency fluorescence quenching. Based on resonance energy transfer from the RBITC molecules to the localized surface plasmon of AuNPs, a linear Stern−Volmer relationship describing the dynamic quenching effect between AuNP concentrations and RBITC fluorescence intensity should be obtained by eq 1, where $F_0$ and $F$ are emission intensity of RBITC in

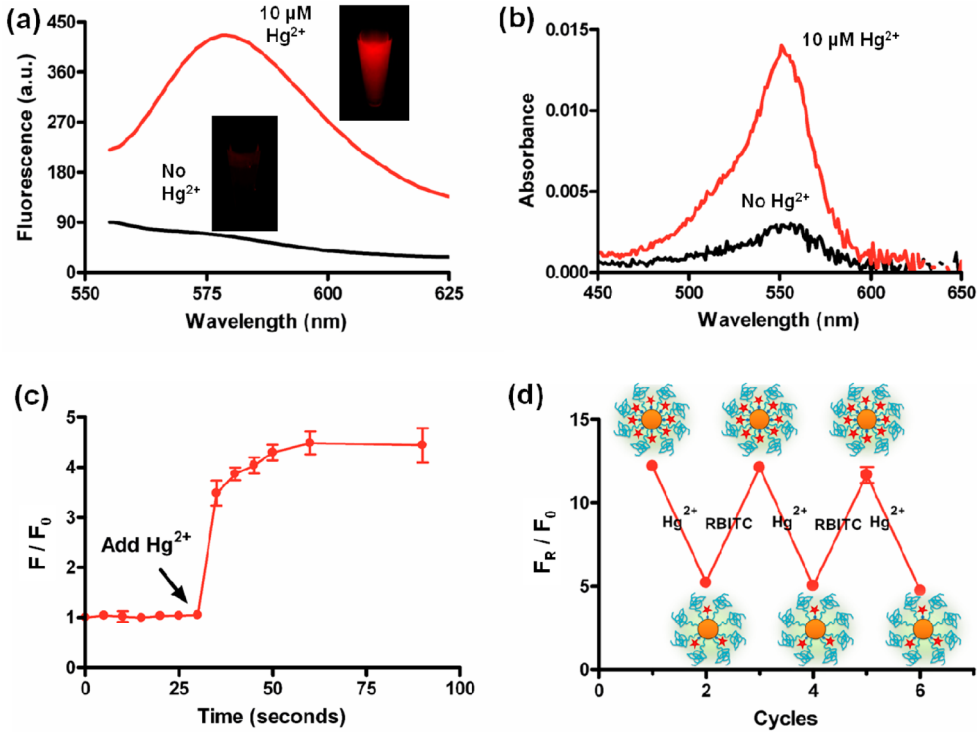


**Figure 4. (a) Fluorescence emission spectra and photograph (inset) of the RBITC-PEG-AuNPs solutions (2.5 nM) before and after addition of 10 $\mu$M of $Hg^{2+}$ ions, and (b) their corresponding UV−vis spectra of released RBITC after centrifugation. (c) Plot of $F/F_0$ values versus time upon the addition of 10 $\mu$M of $Hg^{2+}$ ions into RBITC-PEG-AuNPs solution. ($F$ and $F_0$ are fluorescence intensity at 580 nm in the presence and absence of $Hg^{2+}$). The arrow indicates the starting time of $Hg^{2+}$ addition. (d) $F_R/F_0$ values of RBITC-PEG-AuNPs solutions after incubation with $Hg^{2+}$ and free RBITC alternatively. $F_R$ represents the fluorescence intensity of the remaining RBITC left on the RBITC-PEG-AuNPs (released by 100 mM of DTT) while $F_0$ represents the fluorescence intensity of RBITC-PEG-AuNPs.**

the absence and presence of quencher, respectively; $K_{SV}$ is the Stern−Volmer quenching constant; [Q] is the concentration of the AuNP quencher.[35]

$$\frac{F}{F_0} = 1 + K_{sv}[Q] \quad (1)$$

From the results plotted in Figure 3, however, we observed that the relationship between concentrations of AuNP quencher and $F/F_0$ values was not linear but rather showed an upward deviation from linearity. This effect can be characterized by the combined effects of static quenching, based on the direct binding and association of dyes and AuNPs, and dynamic quenching described above. When taking both quenching effects into account, the quencher concentration factor is no longer in a linear relationship with the fluorescence intensities but rather a squared factor, leading to the extended Stern−Volmer relation:[36]

$$\frac{F}{F_0} = (1 + k_q\tau_0[Q])(1 + k_a[Q]) \quad (2)$$

$$= 1 + k_a[Q] + k_q\tau_0[Q] + k_qk_a\tau_0[Q]^2 \quad (3)$$

where $k_q$ is the bimolecular quenching rate constant; $\tau_0$ is the excited state lifetime in the absence of quencher; $k_a$ is the association constant of RBITC with AuNPs. We reason that the upward curvature of $F_0/F$ versus [Q] plots is most likely associated with the superquenching efficiency of AuNP, which arises from the efficient energy transfer from the RBITC donor to the AuNP acceptor. The AuNP acceptor has a large surface-to-volume ratio and an isotropic distribution of dipole vectors to accept the energy from RBITC. In the case of resonant excitation of surface plasmons on AuNPs, a small dipole in the excited RBITC can lead to a large dipole in the AuNP acceptor, resulting in the superquenching efficiencies.

Next, we measured the fluorescence of RBITC-PEG-AuNPs before and after adding $Hg^{2+}$. In the presence of $Hg^{2+}$ (10 $\mu$M), the attached RBITC molecules were released from AuNP surfaces, and thus the quenched fluorescence of the attached RBITC on AuNPs recovered significantly (Figure 4a). The fluorescence enhancement was observed in a few seconds after the addition of $Hg^{2+}$ (10 $\mu$M). The released RBITC was separated by centrifugation and measured using UV−vis spectroscopy. After separation, we observed the remarkable emergence of an absorption peak at around 555 nm, indicating that $Hg^{2+}$ had the capacity of removing RBITC from AuNP surfaces. On the other hand, without addition of $Hg^{2+}$, there was very weak absorbance at the same absorption band (Figure 4b).

To better understand the response rate of the fluorescence recovery upon addition of $Hg^{2+}$, we measured the changes of fluorescence intensities at different time intervals by testing the $F/F_0$ values (the ratio of fluorescence intensity at 580 nm in the presence and absence of $Hg^{2+}$). We found that, with the addition of $Hg^{2+}$ (the arrow indicates the starting time of $Hg^{2+}$ addition), $F/F_0$ values increased significantly in 1 min and then remained constant with time (Figure 4c). The results revealed that the displacement reaction can be completed quickly, providing a rapid means to determine $Hg^{2+}$.

Interestingly, RBITC-PEG-AuNPs can be regenerated by addition of free RBITC into the AuNPs solutions that were already used for detecting $Hg^{2+}$ and where RBITC was partially released by $Hg^{2+}$. We reasoned that the freshly added RBITC can bind with the remaining active sites of gold left by the released RBITC. To this study, we first treated RBITC-PEG-AuNPs with $Hg^{2+}$, which we have shown displaces RBITC from the AuNP conjugates. After removing the released RBITC by centrifugation, we incubated the solutions with 100 mM of Dithiothreitol (DTT), a common agent used for completely replacing ligands from Au surfaces.[37] At this point, any dye removed by DTT indicates the remaining RBITC left on the RBITC-PEG-AuNPs. We compared the $F_R/F_0$ values of the remaining RBITC after adding $Hg^{2+}$ and free RBITC alternatively along with DTT incubation. $F_R$ represents the fluorescence intensity of the remaining RBITC left on the RBITC-PEG-AuNPs while $F_0$ represents the fluorescence intensity of RBITC-PEG-AuNPs. With the addition of $Hg^{2+}$, the remaining RBITC exhibited reduced $F_R/F_0$ values; while addition of free RBITC caused an increase of the $F_R/F_0$ values (Figure 4d). In other words, low amounts of RBITC are left on the AuNP after $Hg^{2+}$ treatment, but this RBITC amount can be replaced onto the RBITC-PEG-AuNP conjugates by simply resupplying the AuNPs with RBITC molecules. Neither the addition of $Hg^{2+}$ nor the subsequent resupplying of RBITC can induce the aggregation of RBITC-PEG-AuNPs, which was confirmed by the TEM images (Figure S10, Supporting Information). The results indicate that this probe is robust and recyclable, making it particularly useful in remote areas.

We then studied the selectivity of this nanosensor for $Hg^{2+}$ by testing the fluorescence responses to other environmentally relevant metallic ions, including $Ag^{+}$, $Al^{3+}$, $Ba^{2+}$, $Ca^{2+}$, $Cd^{2+}$, $Co^{2+}$, $Cr^{2+}$, $Cu^{2+}$, $Fe^{2+}$, $Fe^{3+}$, $K^{+}$, $Mg^{2+}$, $Mn^{2+}$, $Na^{+}$, $Ni^{2+}$, $Pb^{2+}$ and $Zn^{2+}$ (Figure 5), each with a concentration of 100 $\mu$M. Only $Hg^{2+}$ (10 $\mu$M) induced a noticeable fluorescence recovery of RBITC. As we expected, none of the competing metallic ions interfered with the detection even at increased concentrations up to mM levels. In the control experiments, all metallic ions did not influence the fluorescence of free RBITC, indicating that the enhanced

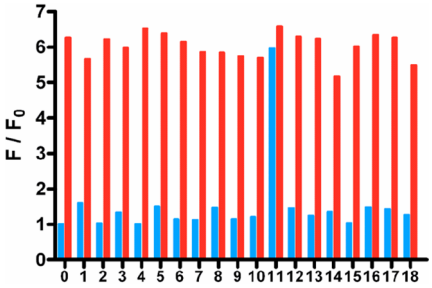


**Figure 5. Selectivity of this assay for $Hg^{2+}$ ions in aqueous solutions. Blue bars indicate the fluorescence recovery of RBITC-PEG-AuNPs solutions (2.5 nM) with addition of 100 $\mu$M metal ions of interest: (0) RBITC-PEG-AuNPs solution, (1) $Ag^{+}$, (2) $Al^{3+}$, (3) $Ba^{2+}$, (4) $Ca^{2+}$, (5) $Cd^{2+}$, (6) $Co^{2+}$, (7) $Cr^{2+}$, (8) $Cu^{2+}$, (9) $Fe^{2+}$, (10) $Fe^{3+}$, (11)$Hg^{2+}$, (12) $K^{+}$, (13) $Mg^{2+}$, (14) $Mn^{2+}$, (15) $Na^{+}$, (16) $Ni^{2+}$, (17) $Pb^{2+}$ and (18) $Zn^{2+}$. Red bars represent the eventual fluorescence recovery after addition of 10 $\mu$M $Hg^{2+}$ ions to each solution containing other metal ions.**

fluorescence of the solution is only due to the $Hg^{2+}$-induced departing of RBITC from AuNP surfaces and thus fluorescence recovery. When the competing metallic ions were mixed with $Hg^{2+}$, the solutions had similar behavior to that containing pure $Hg^{2+}$, that is, inducing remarkable fluorescence enhancement. This result means that the coexistence of various competing metallic ions would not influence the selectivity of this assay. Unlike many fluorescent assays for $Hg^{2+}$, which depend on the addition of masking agents and/or require pretreatment to improve selectivity, our designed probe, does not require any extra agents.

Next, we investigated the sensitivity of this assay for $Hg^{2+}$ in aqueous solutions. We first prepared the solutions containing various concentrations of $Hg^{2+}$ ranging from 0 to 10 $\mu$M. Later, aliquots of the as-prepared RBITC-PEG-AuNP pellets were added into the $Hg^{2+}$ solutions. The eventual concentration of RBITC-PEG-AuNPs in each solution was determined to be 2.5 nM by UV–vis spectroscopy. We allowed the resulting solutions to incubate at room temperature for 1 min and then recorded the fluorescence of RBITC for each solution. We noted that the levels of fluorescence recovery highly depended on the concentration of $Hg^{2+}$, where higher concentrations of $Hg^{2+}$ led to stronger fluorescence recovery. As shown in Figure 6, with the increase of $Hg^{2+}$ concentration, the fluorescence intensities at 580 nm increased gradually. The changes in fluorescence spectra were quantified by measuring the plots of $F/F_0$ values versus the concentrations of $Hg^{2+}$. We found the $F/F_0$ values were linear with the $Hg^{2+}$ concentrations within a range from 10 to 500 nM. The limit of detection (LOD) of this assay is 2.3 nM at a signal-to-noise ratio of 3. This value is particularly attractive because it is lower than the maximum level (10 nM) of $Hg^{2+}$ in drinking water guided by the United States Environmental Protection Agency (EPA)[38] as well as that (30 nM)

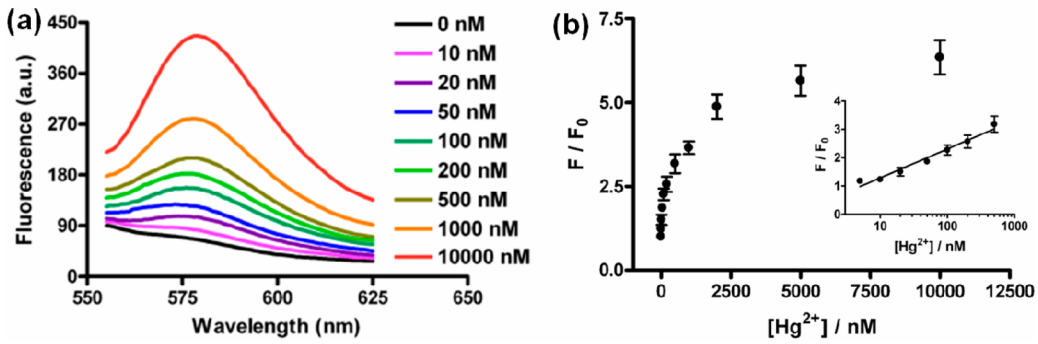


**Figure 6. Sensitivity of this assay for $Hg^{2+}$ ions by fluorescence recovery. (a) Fluorescence emission spectra of the RBITC-PEG-AuNPs solutions (2.5 nM) after addition of varying $Hg^{2+}$ ions from 0 to $10^{-5}$ M. (b) Plot of the fluorescence intensity at 580 nm versus various concentrations of $Hg^{2+}$ ions in the RBITC-PEG-AuNPs solutions.**

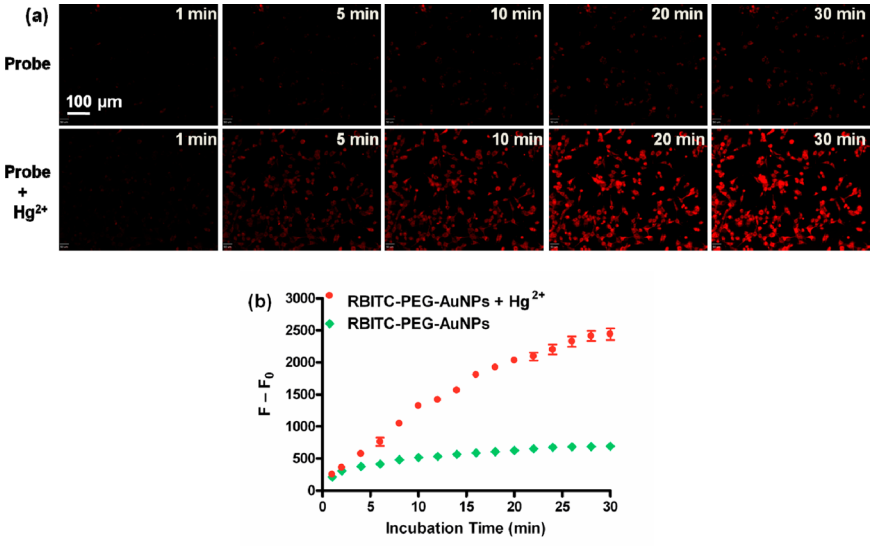


**Figure 7. (a) Intracellular fluorescence at different incubation times. MDA-MB-435 cells were cultured in 8-well plates in the absence (top) and presence (bottom) of 10 $\mu$M $Hg^{2+}$, and RBITC-PEG-AuNPs (20 nM) were added in the medium. The intracellular fluorescence increased over time, which was quantified by the $F-F_0$ values (b). $F$ is the mean fluorescence intensity of RBITC inside cells, and $F_0$ is the background fluorescence.**

permitted by the World Health Organization (WHO).[39]

Although many nanosensors show great potential in bioanalysis with ultrahigh sensitivity, they only work well under specific conditions such as in pure water and are thus unavailable in complex samples. Encouraged by the excellent stability of RBITC-PEG-AuNPs in various complex solutions as well as the extraordinary selectivity and sensitivity of this probe in pure water, we next evaluated if this probe can be used to monitor $Hg^{2+}$ in real environmental samples. First, a water sample from the Potomac River near Washington, D.C. was collected and filtered through a 22 $\mu$m membrane to remove any insoluble substrates. The river water samples were spiked with varying concentrations of $Hg^{2+}$ to evaluate the interference of unknown substances in the river water on the detection. The final concentrations of $Hg^{2+}$ in the river water samples were set to be 0, 10, 20, 40, 80, 150, and 300 nM (1 mL of each concentration). The $Hg^{2+}$-spiked solutions were mixed with the as-prepared RBITC-PEG-AuNP pellets, of which the eventual concentration of AuNPs was 2.5 nM. We observed that the pellets were easily dispersed, and all the solutions remained red, demonstrating proper dispersion of RBITC-PEG-AuNPs in the $Hg^{2+}$-spiked solutions. Next, we measured the fluorescence recovery of each solution. As shown in Figure S11, Supporting Information, the fluorescence intensity increased with the increase of the added $Hg^{2+}$ concentration. The LOD at a signal-to-noise ratio of 3 for the added $Hg^{2+}$ in the river water sample is determined to be 3.8 nM, which is close to that in pure water. The results indicated that the unknown matrices in river water have a negligible effect on the stability and detection of this probe. We suggest that this assay has the capability in monitoring environmentally relevant concentrations of $Hg^{2+}$.

To further investigate the possibility of using this displacement assay for monitoring $Hg^{2+}$ levels in

organisms, we used this assay to detect the intracellular $Hg^{2+}$ in living cells. MDA-MB-435 cells were first incubated with 10 $\mu$M of $Hg^{2+}$ for 0.5 h, and then RBITC-PEG-AuNPs (20 nM) in the medium were added for another 0.5 h incubation. We observed that the fluorescence inside the living cells enhanced gradually, while those without the pretreatment of $Hg^{2+}$ showed very weak intracellular fluorescence (Figure 7a). The enhancement of fluorescence intensity was quantified by the $F-F_0$ values, where $F$ is the mean fluorescence intensity of RBITC inside cells, and $F_0$ is the background fluorescence (Figure 7b). The results revealed that our assay can be used to monitor intracellular $Hg^{2+}$ in living cells. Additionally, bright-field measurements showed that the cells after treatment with $Hg^{2+}$ (10 $\mu$M) and RBITC-PEG-AuNPs (20 nM) were still viable during the imaging (Figure S12, Supporting Information). We performed MTT experiments to explore the cytotoxicity of RBITC-PEG-AuNPs. The results showed that the cell viability was between 95−100% after incubation of various concentrations of RBITC-PEG-AuNPs ranging from 0 to 80 nM with cells for 24 h (Figure S13, Supporting Information). This indicates that the probe does not affect the cell viability, making this probe particularly suitable for $Hg^{2+}$ detection in biological samples.

## CONCLUSION

In conclusion, we present a very robust, recyclable, inexpensive, ultrasensitive and selective gold nanoparticle-based NSET probe for monitoring $Hg^{2+}$ levels in aqueous solutions and living cells. On the basis of our rational design, this assay was endowed with extraordinary selectivity for $Hg^{2+}$ over competing analytes. Unlike many nanomaterial-based probes, the RBITC-PEG-AuNPs, described in this manuscript, remained well-dispersed in complex samples such as river water, tap water, and biological fluids, providing a novel means to screen $Hg^{2+}$ levels in various real samples. Importantly, the sensitivity of this assay (2.3 nM) for $Hg^{2+}$ in aqueous media is higher than both the EPA and the WHO standard limits. Furthermore, this probe can be recyclable and the detection can be completed in 1 min, enabling this assay for $Hg^{2+}$ monitoring not only in developed areas but also in remote areas with limited resources. We believe that this AuNP-based displacement assay is a promising point-of-care device to be used in many settings, especially in combination with other formats such as lab-on-chip and microfluidic devices.[40−43]

## EXPERIMENTAL SECTION

**Materials and Instrumentation.** Chemicals such as Rhodamine B isothiocyanate (RBITC), Poly(ethylene glycol) (PEG) 2000, $HAuCl_4\cdot 3H_2O$, trisodium citrate, and metallic salts ($AgNO_3$, $Al(NO_3)_3\cdot 9H_2O$, $Ba(NO_3)_2$, $CaCl_2$, $Cd(SO_4)\cdot 8H_2O$, $CoCl_2\cdot 6H_2O$, $Cr(NO_3)_3\cdot 9H_2O$, $Cu(NO_3)_2\cdot 3H2O$, $Fe(NO_3)_2\cdot 6H_2O$, $Fe(NO_3)_3\cdot 9H_2O$, $Hg(ClO_4)_2\cdot 3H_2O$, $KNO_3$, $MgSO_4$, $MnSO_4\cdot 2H_2O$, NaNO3, $Ni(NO_3)_2\cdot 6H_2O$, $Pb(NO_3)_2$, $Zn(NO_3)_2\cdot 6H_2O$) were purchased from major suppliers such as Sigma-Aldrich and Alfa Aesar and used as received. Distilled water was used throughout the work. The UV−vis spectra of gold colloidal solutions and Rhodamine B isothiocyanate (RBITC) solutions were recorded with a Genesys 10s UV−vis spectrophotometer. The fluorescence spectra were collected using an F-7000 fluorescence spectrophotometer (Hitachi, Tokyo, Japan) operating at an excitation wavelength at 530 nm, excitation and emission slit widths were 5 and 5 nm, respectively. The fluorescence intensities were collected at 580 nm. We used the emission fluorescence value over the initial emission fluorescence value ($F/F_0$) to measure the variations of the fluorescence intensity. Dynamic light scattering (DLS) and zeta potential ($\zeta$) were performed on a Zeta Sizer Nano ZS (Malvern Zetasizer 3000HS and He/Ne laser at 632.8 nm and scattering angles of 90 at 25 °C). TEM images were obtained by using a JEOL1400 model at an accelerating voltage of 100 kV.

**Preparation of RBITC-AuNPs.** The synthesis of citrate-AuNPs (13 nm) has been reported elsewhere.[15,16,21] In brief, a stirred aqueous solution of $HAuCl_4$ (41 mg, 1.0 mM) in 100 mL water was heated to reflux, and a trisodium citrate solution (114 mg, 38.8 mM) dissolved in hot water (10 mL) was added. The solution was heated under reflux with vigorous stirring for another 15 min, its color changed from pale yellow to deep red. The solution was cooled to room temperature with a slow and continuous stirring. The resulting solution was filtered with a PES membrane (filter unit is 22 $\mu$m) to remove some large clusters and insoluble compounds. The sizes of the nanoparticles were about 13 nm by TEM analysis, the corresponding absorption band is at ~520 nm.

To prepare RBITC-PEG-AuNPs, the pH value of the as-prepared citrate-AuNPs solution (2.5 nM, 1 mL) was adjusted by $K_2CO_3$ (100 mM) to be 8. A stock solution of RBITC (10 mM, 1 $\mu$L) was added into the citrate-AuNPs solution (2.5 nM, 1 mL) with vigorous shaking to allow adsorption of RBITC to the AuNP surface. The resulting solution was shaken (600 r/min) in the dark at room temperature for 1 h for sufficient equilibration. Later, PEG (1 mM, 3 $\mu$L) was added into the solution of RBITC-AuNPs and agitated for 10 min at room temperature. The excess RBITC and PEG were removed by three runs of centrifugation (14000 r/min, 15 min) and the AuNP pellets were obtained and stored at 4 °C for further use. The fluorescence spectra of the RBITC-PEG-AuNPs solutions were measured with excitation at 530 nm. The decrease of the fluorescence of RBITC-PEG-AuNPs solutions indicated that RBITC molecules had adsorbed onto the surfaces of AuNPs and the fluorescence of RBITC was dramatically quenched by AuNPs.

**Experimental Procedures for Detection of $Hg^{2+}$ in Aqueous Solutions.** A typical detection procedure for $Hg^{2+}$ was performed as follows. A stock solution of $Hg^{2+}$ was serially diluted with distilled water for various folds. The volume for each $Hg^{2+}$ solution was 1 mL. Aliquots of the as-prepared RBITC-PEG-AuNP pellets were mixed with the different concentrations of $Hg^{2+}$ solutions. The resulting mixtures were kept in the dark for 1 min, and then the fluorescence for each solution was measured at room temperature. All the measurements were repeated 3 times for each concentration.

To investigate the selectivity of this assay, 0.1 mmol of each kind of metal ions ($Ag^+$, $Al^{3+}$, $Ba^{2+}$, $Ca^{2+}$, $Cd^{2+}$, $Co^{2+}$, $Cr^{2+}$, $Cu^{2+}$, $Fe^{2+}$, $Fe^{3+}$, $Hg^{2+}$, $K^+$, $Mg^{2+}$, $Mn^{2+}$, $Na^+$, $Ni^{2+}$, $Pb^{2+}$ and $Zn^{2+}$) was dissolved in distilled water (1 mL) to afford 100 mM aqueous solution. The stock solutions were diluted to desired concentrations with distilled water when needed. Typically, 1 mL of each metallic salt (100 $\mu$M) was incubated with aliquots of the as-prepared RBITC-PEG-AuNP pellets, after 1 min incubation, the fluorescence intensities of the resulting solutions were measured and analyzed.

To evaluate the potential of this assay in practical applications, we collected river water from the Potomac River near Washington, D.C. and used as real samples. The river water was

filtered by using a PES membrane (filter unit is 0.22 $\mu$m) to remove the insoluble materials, and then spiked with different volumes of $Hg^{2+}$ stock solutions to result in final concentrations of $Hg^{2+}$ to be: 0, 10, 20, 40, 80, 150, and 300 nM (1 mL of each concentration). The spiked river water containing varying concentrations of $Hg^{2+}$ was mixed with the RBITC-PEG-AuNP pellets, and the fluorescence for each solution was recorded after 1 min of incubation in the dark.

**Cell Culture.** Human breast carcinoma malignant cell line (MDA-MB-435) was cultured in L-15 medium (GIBCO) supplemented with 10% fetal bovine serum (GIBCO) and 1% penicillin/streptomycin sulfate (antibiotic, GIBCO), and maintained at 37 °C in a humidified 5% $CO_2$ atmosphere. Before seeding, cells were washed with PBS, dissociated from culture plates with trypsin/EDTA (GIBCO), and resuspended in L-15 medium containing 10% FBS. After centrifugation at 800 rpm for 3 min, the cell pellet was resuspended in L-15 medium containing 10% of FBS (cell density is about $1 \times 10^4$/well).

**Cell Imaging Methods.** MDA-MB-435 cells were seeded in 8-well plates and cultured overnight. After cell attachment, the wells were washed with fresh medium three times and then 10 $\mu$M of $Hg^{2+}$ in PBS were added and incubated for 30 min at room temperature. After another round of washing with medium three times, the $Hg^{2+}$-treated cells were incubated with the RBITC-PEG-AuNPs solutions (20 nM) in fresh medium, then the fluorescence imaging of intracelluar $Hg^{2+}$ was observed by RFP filter under an Olympus IX81 microscope. Time-lapse images were acquired at 1 min intervals for 0.5 h with 10× objective lens. The MDA-MB-435 cells without the pretreatment of $Hg^{2+}$ were set as a control. For all fluorescence images, the microscope settings such as brightness, contrast, and exposure time were held constant to compare the relative intensity of intracellular $Hg^{2+}$ fluorescence.

**Cytotoxicity.** The cytotoxicity of RBITC-PEG-AuNPs was investigated using the standard MTT assay protocol. In brief, MDA-MB-435 cells were incubated with various concentrations of RBITC-PEG-AuNPs (0, 1.25, 2.5, 5, 10, 20, 40, 80 nM) in medium for 24 h. The medium was replaced with 200 $\mu$L fresh media containing 20 $\mu$L of MTT solution (5 mg/mL), and the incubation proceeded for 4 h. The media was then removed, and 150 $\mu$L of dimethyl sulfoxide (DMSO) was added into each well to dissolve the internalized purple formazan crystals. An aliquot of 100 $\mu$L of solution in each well was transferred into a new 96-well plate. The absorbance at 570 nm was recorded using a microplate reader. The absorbance from the control cells was set as 100% cell viability.

*Conflict of Interest:* The authors declare no competing financial interest.

*Acknowledgment.* This work was supported in part, by the National Basic Research Program of China (973 program) (973 Program No. 2013CB733802, 2013CB733800), the National Science Foundation of China (NSFC) (81101101, 51273165, 51173117, 50830107, 81171399, and 81101077), the National Significant New Drugs Creation Program (2012ZX09505-001-001), the Jiangsu Province Social Development Program (BE2012622 and BL2012031), the Outstanding Professional Fund of Health Ministry in Jiangsu Province (RC2011095), the Chinese Academy of Sciences professorship for Senior International Scientists (2011T2J06), and the Intramural Research Program (IRP) of the National Institute of Biomedical Imaging and Bioengineering (NIBIB), National Institutes of Health (NIH).

*Supporting Information Available:* Details of DLS measurements, UV–vis and fluorescence emission spectra, and TEM Images of various AuNP formulas. Fluorescence microscope images of MDA-MB-435 cells treated with $Hg^{2+}$ and RBITC-PEG-AuNPs. This material is available free of charge via the Internet at http://pubs.acs.org.

## REFERENCES AND NOTES

1. Bolger, P. M.; Schwetz, B. A. Mercury and Health. *N. Engl. J. Med.* **2002**, *347*, 1735–1736.
2. Clarkson, T. W.; Magos, L.; Myers, G. J. The Toxicology of Mercury-Current Exposures and Clinical Manifestations. *N. Engl. J. Med.* **2003**, *349*, 1731–1737.
3. Onyido, I.; Norris, A. R.; Buncel, E. Biomolecule-Mercury Interactions: Modalities of DNA Base-Mercury Binding Mechanisms. Remediation Strategies. *Chem. Rev.* **2004**, *104*, 5911–5929.
4. Erxleben, H.; Ruzicka, J. Atomic Absorption Spectroscopy for Mercury, Automated by Sequential Injection and Miniaturized in Lab-on-Valve System. *Anal. Chem.* **2005**, *77*, 5124–5128.
5. Jia, X. Y.; Gong, D. R.; Han, Y.; Wei, C.; Duan, T. C.; Chen, H. T. Fast Speciation of Mercury in Seawater by Short-Column High-Performance Liquid Chromatography Hyphenated to Inductively Coupled Plasma Spectrometry after On-line Cation Exchange Column Preconcentration. *Talanta* **2012**, *88*, 724–729.
6. Leermakers, M.; Baeyens, W.; Quevauviller, P.; Horvat., M. Mercury in Environmental Samples: Speciation, Artifacts and Validation. *Trends Anal. Chem.* **2005**, *24*, 383–393.
7. Huang, J. H.; Xu, Y. F.; Qian, X. H. A Rhodamine-Based $Hg^{2+}$ Sensor with High Selectivity and Sensitivity in Aqueous Solution: A NS2-Containing Receptor. *J. Org. Chem.* **2009**, *74*, 2167–2170.
8. Kim, I. B.; Bunz, U. H. F. Modulating the Sensory Response of a Conjugated Polymer by Proteins: An Agglutination Assay for Mercury Ions in Water. *J. Am. Chem. Soc.* **2006**, *128*, 2818–2819.
9. Ono, A.; Togashi, H. Highly Selective Oligonucleotide-Based Sensor for Mercury(II) in Aqueous Solutions. *Angew. Chem., Int. Ed.* **2004**, *43*, 4300–4302.
10. Chen, P.; He, C. A General Strategy to Convert the MerR Family Proteins into Highly Sensitive and Selective Fluorescent Biosensors for Metal Ions. *J. Am. Chem. Soc.* **2004**, *126*, 728–729.
11. Yun, C. S.; Javier, A.; Jennings, T.; Fisher, M.; Hira, S.; Peterson, S.; Hopkins, B.; Reich, N. O.; Strouse, G. F. Nanometal Surface Energy Transfer in Optical Rulers, Breaking the FRET Barrier. *J. Am. Chem. Soc.* **2005**, *127*, 3115–3119.
12. Bunz, U. H. F.; Rotello, V. M. Gold Nanoparticle-Fluorophore Complexes: Sensitive and Discerning "Noses" for Biosystems Sensing. *Angew. Chem., Int. Ed.* **2010**, *49*, 3268–3279.
13. Dulkeith, E.; Ringler, M.; Klar, T. A.; Feldmann, J.; Muñoz Javier, A.; Parak, W. J. Gold Nanoparticles Quench Fluorescence by Phase Induced Radiative Rate Suppression. *Nano Lett.* **2005**, *5*, 585–589.
14. Swierczewska, M.; Lee, S.; Chen, X. The Design and Application of Fluorophore–Gold Nanoparticle Activatable Probes. *Phys. Chem. Chem. Phys.* **2011**, *13*, 9929–9941.
15. Darbha, G. K.; Ray, A.; Ray, P. C. Gold Nanoparticle-Based Miniaturized Nanomaterial Surface Energy Transfer Probe for Rapid and Ultrasensitive Detection of Mercury in Soil, Water, and Fish. *ACS Nano* **2007**, *1*, 208–214.
16. Huang, C. C.; Chang, H. T. Selective Gold-Nanoparticle-Based "Turn-On" Fluorescent Sensors for Detection of Mercury(II) in Aqueous Solution. *Anal. Chem.* **2006**, *78*, 8332–8338.
17. Liu, D. B.; Chen, W. W.; Wei, J. H.; Li, X. B.; Wang, Z.; Jiang, X. Y. A Highly Sensitive, Dual-Readout Assay Based on Gold Nanoparticles for Organophosphorus and Carbamate Pesticides. *Anal. Chem.* **2012**, *84*, 4185–4191.
18. Liu, D. B.; Chen, W. W.; Tian, Y.; He, S.; Zheng, W. F.; Sun, J. S.; Wang, Z.; Jiang, X. Y. A Highly Sensitive Gold-Nanoparticle-Based Assay for Acetylcholinesterase in Cerebrospinal Fluid of Transgenic Mice with Alzheimer's Disease. *Adv. Healthcare Mater.* **2012**, *1*, 90–95.
19. Chen, J. L.; Zheng, A. F.; Chen, A. H.; Gao, Y. C.; He, C. Y.; Kai, X. M.; Wu, G. H.; Chen, Y. C. A Functionalized Gold Nanoparticles and Rhodamine 6G Based Fluorescent Sensor for High Sensitive and Selective Detection of Mercury(II) in Environmental Water Samples. *Anal. Chim. Acta* **2007**, *599*, 134–142.
20. De, M.; Rana, S.; Akpinar, H.; Miranda, O. R.; Arvizo, R. R.; Bunz, U. H. F.; Rotello, V. M. Sensing of Proteins in Human Serum Using Conjugates of Nanoparticles and Green Fluorescent Protein. *Nat. Chem.* **2009**, *1*, 461–465.
21. Liu, D. B.; Wang, Z.; Jiang, X. Y. Gold Nanoparticles for the Colorimetric and Fluorescent Detection of Ions and Small Organic Molecules. *Nanoscale* **2011**, *3*, 1421–1433.

22. Smith, R. M.; Martell, A. E. *Critical Stability Constants*; Plenum Press: New York, 1976; Vol. 4: Inorganic complexes.
23. Liu, D. B.; Qu, W. S.; Chen, W. W.; Zhang, W.; Wang, Z.; Jiang, X. Y. Highly Sensitive, Colorimetric Detection of Mercury(II) in Aqueous Media by Quaternary Ammonium Group-Capped Gold Nanoparticles at Room Temperature. *Anal. Chem.* **2010**, *82*, 9606–9610.
24. Qian, X. M.; Emory, S. R.; Nie, S. M. Anchoring Molecular Chromophores to Colloidal Gold Nanocrystals: Surface-Enhanced Raman Evidence for Strong Electronic Coupling and Irreversible Structural Locking. *J. Am. Chem. Soc.* **2012**, *134*, 2000–2003.
25. Hammock, M. L.; Sokolov, A. N.; Stoltenberg, R. M.; Naab, B. D.; Bao, Z. Organic Transistors with Ordered Nanoparticle Arrays as a Tailorable Platform for Selective, *In Situ* Detection. *ACS Nano* **2012**, *6*, 3100–3108.
26. Liu, D. B.; Chen, W. W.; Sun, K.; Deng, K.; Zhang, W.; Wang, Z.; Jiang, X. Y. Resettable, Multi-Readout Logic Gates Based on Controllably Reversible Aggregation of Gold Nanoparticles. *Angew. Chem., Int. Ed.* **2011**, *50*, 4103–4107.
27. Kumar, A. S.; Ye, T.; Takami, T.; Yu, B. C.; Flatt, A. K.; Tour, J. M.; Weiss, P. S. Reversible Photo-Switching of Single Azobenzene Molecules in Controlled Nanoscale Environments. *Nano Lett.* **2008**, *8*, 1644–1648.
28. Joshi, P.; Chakraborti, S.; Ramirez-Vick, J. E.; Ansari, Z. A.; Shanker, V.; Chakrabarti, P.; Singh, S. P. The Anticancer Activity of Chloroquine-Gold Nanoparticles against MCF-7 Breast Cancer Cells. *Colloids Surf. B* **2012**, *95*, 195–200.
29. Ding, Y.; Chen, Z.; Xie, J.; Guo, R. Comparative Studies on Adsorption Behavior of Thionine on Gold Nanoparticles with Different Sizes. *J. Colloid Interface Sci.* **2008**, *327*, 243–250.
30. Narband, N.; Uppal, M.; Dunnill, C. W.; Hyett, G.; Wilsonb, M.; Parkin, I. P. The Interaction between Gold Nanoparticles and Cationic and Anionic Dyes: Enhanced UV-visible Absorption. *Phys. Chem. Chem. Phys.* **2009**, *11*, 10513–10518.
31. Ojea-Jiménez, I.; López, X.; Arbiol, J.; Puntes, V. Citrate-Coated Gold Nanoparticles As Smart Scavengers for Mercury(II) Removal from Polluted Waters. *ACS Nano* **2012**, *6*, 2253–2260.
32. Rostro-Kohanloo, B. C.; Bickford, L. R.; Payne, C. M.; Day, E. S.; Anderson, L. J. E.; Zhong, M.; Lee, S.; Mayer, K. M.; Zal, T.; Adam, L.; et al. The Stabilization and Targeting of Surfactant-Synthesized Gold Nanorods. *Nanotechnology* **2009**, *20*, 434005.
33. Lipka, J.; Semmler-Behnke, M.; Sperling, R. A.; Wenk, A.; Takenaka, S.; Schleh, C.; Kissel, T.; Parak, W. J.; Kreyling, W. G. Biodistribution of PEG-Modified Gold Nanoparticles Following Intratracheal Instillation and Intravenous Injection. *Biomaterials* **2010**, *31*, 6574–6581.
34. Liopo, A.; Conjusteau, A.; Tsyboulski, D.; Ermolinsky, B.; Kazansky, A.; Oraevsky, A. Biocompatible Gold Nanorod Conjugates for Preclinical Biomedical Research. *J. Nanomed. Nanotechnol.* **2012**, *S2*, 001–010.
35. Fan, C. H.; Wang, S.; Hong, J. W.; Bazan, G. C.; Plaxco, K. W.; Heeger, A. J. Beyond Superquenching: Hyper-Efficient Energy Transfer from Conjugated Polymers to Gold Nanoparticles. *Proc. Natl. Acad. Sci. U.S.A.* **2003**, *100*, 6297–6301.
36. Thipperudrappa, J.; Biradar, D. S.; Hanagodimath, S. M. Simultaneous Presence of Static and Dynamic Component in the Fluorescence Quenching of Bis-MSB by CCl4 and Aniline. *J. Lumin.* **2007**, *1244*, 45–50.
37. Stoeva, S. I.; Lee, J.; Smith, J. E.; Rosen, S. T.; Mirkin, C. A. Multiplexed Detection of Protein Cancer Markers with Biobarcoded Nanoparticle Probes. *J. Am. Chem. Soc.* **2006**, *128*, 8378–8379.
38. U.S. EPA, Mercury Update: Impact on Fish Advisories: EPA-823-F-01-011, 2001. http://water.epa.gov/scitech/swguidance/fishshellfish/outreach/upload/2001_05_31_fish_advice_mercupd.pdf
39. World Health Organization. Guidelines for drinking-water quality: incorporating 1st and 2nd addenda, Vol. 1, Recommendations, 3rd ed.; World Health Organization: Geneva, 2008. http://www.who.int/water_sanitation_health/dwq/fulltext.pdf
40. Zhang, W. H.; Lin, S. C.; Wang, C. M.; Hu, J.; Li, C.; Zhuang, Z. X.; Zhou, Y. L.; Mathies, R. A.; Yang, C. J. PMMA/PDMS Valves and Pumps for Disposable Microfluidics. *Lab Chip* **2009**, *9*, 3088–3094.
41. Hu, M.; Yan, J.; He, Y.; Lu, H. T.; Weng, L. X.; Song, S. P.; Fan, C. H.; Wang, L. H. Ultrasensitive, Multiplexed Detection of Cancer Biomarkers Directly in Serum by Using a Quantum Dot-Based Microfluidic Protein Chip. *ACS Nano* **2010**, *4*, 488–494.
42. Du, Y.; Chen, C. G.; Zhou, M.; Dong, S. J.; Wang, E. K. Microfluidic Electrochemical Aptameric Assay Integrated On-Chip: A Potentially Convenient Sensing Platform for the Amplified and Multiplex Analysis of Small Molecules. *Anal. Chem.* **2011**, *83*, 1523–1529.
43. Xiang, Y.; Lu, Y. Portable and Quantitative Detection of Protein Biomarkers and Small Molecular Toxins Using Antibodies and Ubiquitous Personal Glucose Meters. *Anal. Chem.* **2012**, *84*, 4174–4178.